Influence of precursor concentration solution on CO sensing performance of sprayed nanocrystalline SnO_2 thin films

R. H. BARI*, S. B. PATIL, A. R. BARI[a]
Nanomaterials Research Laboratory, Department of Physics, G. D. M. Arts, K. R. N. Commerce and M.D. Science College, Jamner 424 206, Maharashtra, India
[a]*Department of Physics, Arts, Commerce and Science College, Bodwad 425 310, Maharashtra, India*

Nanocrystalline SnO_2 thin films of different precursor concentration (0.025, 0.05 and 0.075 M) were deposited onto glass substrate at 250^o C by simple spray pyrolysis (SP) technique. These samples were structurally and morphologically characterized using the XRD, FE-SEM techniques, respectively. The SnO_2 films were found to be tetragonal in crystal structure and nanocrystalline in nature. As increase in thickness of films the texture coefficients for plane (110), (101) and (200) were increases. The average crystallite and grain size observed from XRD and FF-SEM was found to be less than 31 and 48 nm respectively. The films sprayed for 0.05M was observed to be most sensitive (S = 180.81) to CO for 100 ppm at 300^{o}C. The sensor shows quick response (3 s) and fast recovery (8 s).

(Received April 24, 2012; accepted September 20, 2012)

Keywords: Spray pyrolysis, Nanocrystalline SnO_2, CO gas sensing, Quick response, Fast recovery

1. Introduction

In recent years, there is an ever-increasing demand for gas sensors in various fields; particular attention has been devoted to the monitoring of carbon monoxide (CO) [1]. SnO_2 gas sensors are among the most reliable options. SnO_2 based semiconductor gas sensors are widely used to measure CO and other reducing gas in the presence of O_2. Only a few studies related to the operation in oxygen free or reducing atmospheres are available [2]. The detection principle is based on a surface reaction between the SnO_2 and the gas to be detected. This reaction modifies the concentration of charge carriers in the semiconductor giving rise to a change in its conductivity [3]. It has also been found that the influence of the film thickness depends on the type of target gas [4, 5].

A variety of techniques have been used to prepare tin oxide (SnO_2) thin films. These include ultrasonic spray pyrolysis [6], chemical vapour deposition [7], activated reactive evaporation [8], ion-beam assisted deposition [9], sputtering [10] and sol–gel [11] methods. Among these techniques, spray pyrolysis has proved to be simple, reproducible and inexpensive, as well as suitable for large area applications. Besides the simple experimental arrangement, high growth rate and mass production capability for large area coatings make them useful for industrial as well as solar cell applications. In addition, spray pyrolysis opens up the possibility to control the film morphology and particle size in the nanometer range.

In the present investigations, nanocrystalline SnO_2 thin films with different precursor concentration of solution were prepared by spray pyrolysis technique. Crystallite size and grain sizes were studied using X-ray diffraction, Field emission scanning electron microscope (FESEM). These nanostructured SnO_2 thin films were tested for sensing different gases and were observed to be most sensitive to CO at 300 ^{O}C.

2. Experimental details

2.1. Substrate cleaning

The substrate cleaning is very important in the deposition of thin films. Commercially available glass slides with a size of 25 mm × 25 mm × 1 mm were washed using soap solution and subsequently kept in hot chromic acid and then cleaned with deionized water followed by rinsing in acetone. Finally, the substrates were previously cleaned with deionized water for 20 min and wiped with acetone and stored in a hot oven.

2.2. Preparation of nanocrystalline SnO_2 thin films

Fig. 1 shows spray pyrolysis technique for preparation of nanocrystalline SnO_2 thin films. Set-up consists of spraying chamber, spray nozzle (gun), compressor for carrier gas, heating system, and temperature indicator.

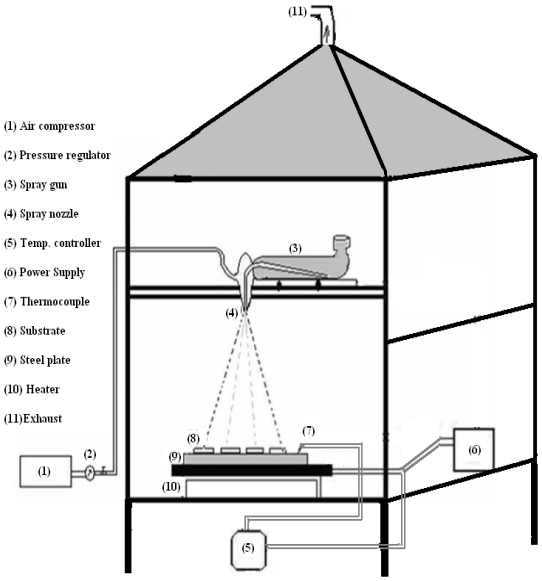

Fig. 1. Schematic diagram of spray pyrolysis system for the preparation of nanocrystalline SnO_2 thin films.

Nanocrystalline tin oxide thin films were prepared by using tin (II) dichloride dihydrate ($SnCl_2.2H_2O$), Purified Merck) in de-ionized water as a precursor. A different concentration of precursor solution (0.025, 0.050, 0.075) was sprayed through a specially designed glass nozzle of 0.5 mm inner diameter onto the ultrasonically cleaned glass substrates. The deposition parameters like substrate temperature (250 ^oC), rate of spraying solution (5 mL/min.), nozzle to substrate distance (30 cm), quantity of the solution sprayed (40 ml), pressure of carrier gas, and to and from movement of the nozzle were kept constant at the optimized values. As prepared nanostructured SnO_2 samples referred as S1, S2 and S3. The pyrolytic reaction takes place on a heated substrate, leading to a poly-crystalline metal oxide. The usual expression for this reaction is:

$$SnCl_2 \cdot 2H_2O \rightarrow SnO_2 + 2H_2 \uparrow + Cl_2 \uparrow \qquad (1)$$

2.3. Annealing of SnO_2 thin films

The as prepared nanocrystalline SnO_2 thin film samples S1, S2, and S3 were annealed at 500^oC for 1 h.

2.4. Sensing system to test the sensor

Fig. 2 shows block diagram of gas sensing system. The gas sensing studies were carried out using a static gas chamber to sense CO gas in air ambient. The nanocrystalline SnO_2 thin films were used as the sensing elements. The sensing element was kept directly on a heater in the gas chamber and the temperature of the heater is controlled by controlling the current passing through the heater. The chromel-alumel (Cr-Al) thermocouple was used in contact with the sensor to sense the operating temperature of the sensor. The output of the thermocouple was connected to a digital temperature indicator. The known volume of the CO gas was introduced into the gas chamber pre-filled with air and it was maintained at atmospheric pressure. A constant voltage was applied to the sensor. And the current was measured by a digital picoammeter.

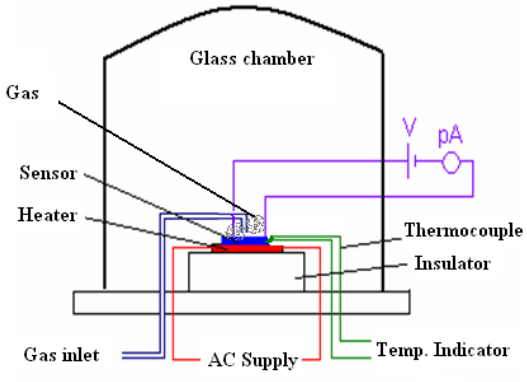

Fig. 2. Block diagram of gas sensing system.

2.5. Thin film characterizations

The nanocrystalline SnO_2 thin film were characterized by X-ray diffraction ((Miniflex Model, Rigaku, Japan)) using CuKα radiation with a wavelength, λ = 1·5418 Å. The microstructure of the films was analyzed using a field emission scanning electron microscope (FE-SEM, JEOL. JED 6300). Electrical and gas sensing properties were measured using a static gas sensing system. The sensor performances were measured on exposure of Liquefied petroleum gas, carbon dioxide, carbon monoxide, hydrogen, ammonia, ethanol, and chlorine was examined.

3. Results

3.1. X-ray diffraction analysis

Fig. 3 shows the X-ray diffractogram of thin film samples S1, S2, and S3. The peaks (110), (101), (200), (211), (220), (310) and (301) in the XRD pattern are match well with the reported ASTM data of pure nanocrystalline SnO_2 [12].

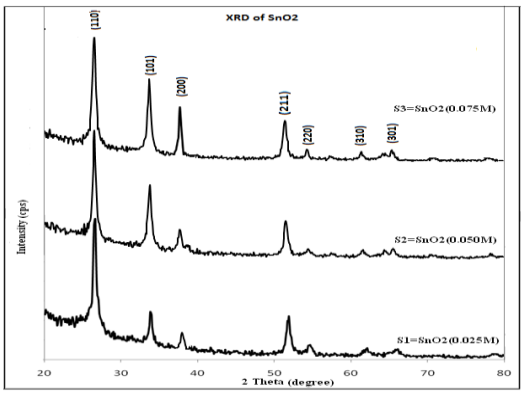

Fig. 3. X-ray diffractogram of nanocrystalline SnO_2 thin films samples: (a) S1, (b) S2, and (c) S3.

These diffraction profiles illustrate crystalline nature and tetragonal structure of SnO_2 thin films. Average crystallite size of nanocrystallite associated with S1, S2, and S3 was calculated using Scherer formula.

$$D = 0{\cdot}9\lambda/\beta\cos\theta \quad (2)$$

Where, D = Average crystallite size
λ = X-ray wavelength (1·542 Å)
β = FWHM of the peak
θ= Diffraction peak position.

The calculated crystallite sizes were presented in Table 1.

3.2. Surface morphology

The microstructure of the prepared film was analyzed using a field emission scanning electron microscope (FE-SEM, JEOL. JED 6300).

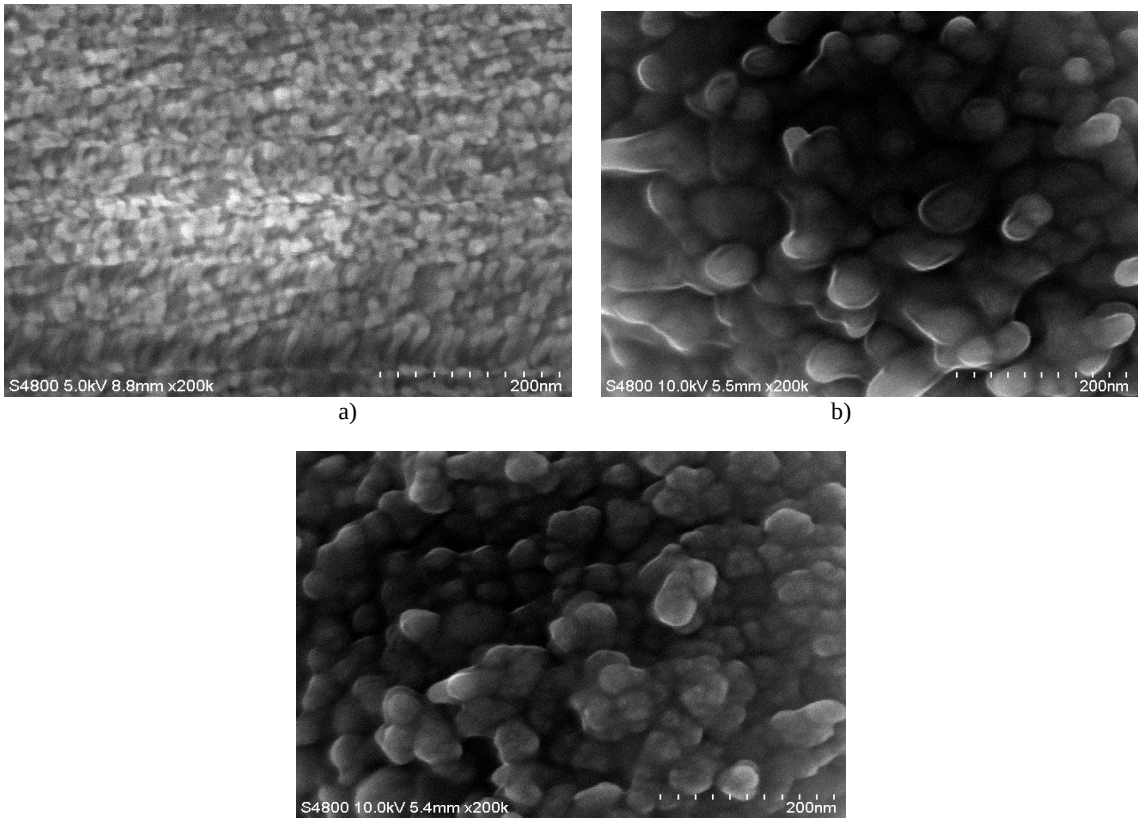

Fig. 4. FESEM images: (a) S1, (b) S2, and (c) S3.

Fig. 4 (a)–(c) shows the FESEM images, showing surface morphology of S1, S2, and S3 thin film samples respectively. The morphology of the grains was roughly spherical in shape. The observed grain sizes were presented in Table 1. Thus the grain size goes on increasing and smoothness goes on decreasing with the increase in precursor concentration of solution.

3.3.1. Determination of film thickness

Film thickness was measured by using a micro gravimetrical method [14] (considering the density of the bulk tin oxide). The films were deposited on clean glass slides whose mass was previously determined. After the deposition the substrate was again weighted, determining the quantity of deposited SnO_2. Measuring the surface area of the deposited film, taking account of SnO_2 specific weight of the film, thickness was determined using the relation:

$$T= M_{SnO2}/A*\rho *10^4 \quad (3)$$

Where A = Surface area of the film [cm^2]
M_{SnO2}= Quantity of the deposited tin oxide
ρ = Specific weight of SnO_2.

The values of the film thickness are given in Table1.

Table 1. Measurement of crystalline size, grain size and film thickness.

Sample	Precursor Concentration (M)	Thickness (nm)	Crystalline size from XRD (nm)	Grain size from FE-SEM (nm)
S1	0.025	180	17	26
S2	0.050	210	23	32
S3	0.075	289	32	39

It is clear from Table 1 that, the thickness of the film was varied from 180 to 289 nm. It was found that the thickness of the film increases, with increase in concentration of the sprayed solution. It is also clear from table that crystallite and grain sizes go on increasing with increase in film thickness.

3.3.2. Variation of texture coefficient with film thickness

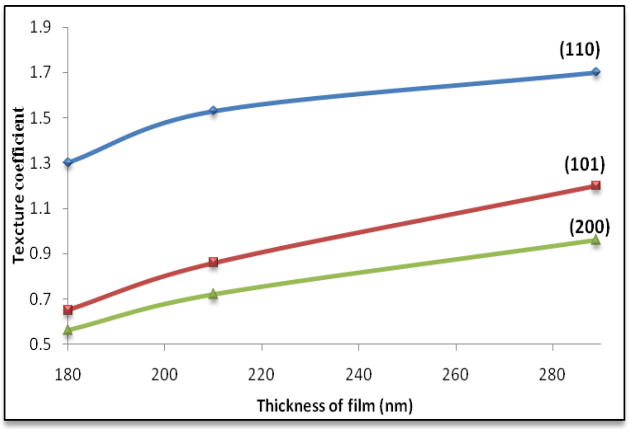

Fig. 5. Variation of texture coefficient with thickness of film.

Fig. 5 shows variation of texture coefficient (TC) with concentration of solution. The formula of texture coefficient (TC) is:

$$TC = \frac{I_{(hkl)}/ I_{0(hkl)}}{(1/N)\,[\Sigma N\, I_{(hkl)}/ I_{0(hkl)}]} \quad (4)$$

Where, I = the measured intensity,
I_0 = the ASTM standard intensity
N = the number of diffraction peaks.

The increase in film thickness (180 nm - 289 nm) results in continuous increase in texture coefficient (TC) for (110), (101) and (200) plane.

3.3.3. Variation of crystallite size with thickness

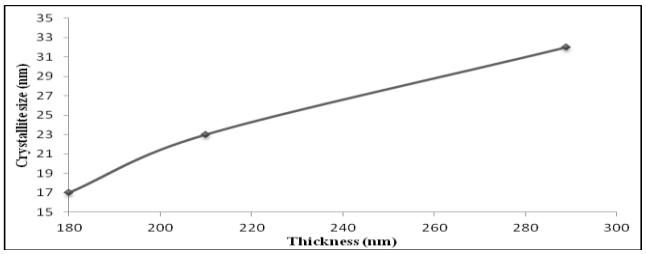

Fig. 6. Variation of crystallite size with thickness of nanocrystalline SnO_2 thin films.

Fig. 6 shows the variation of crystallite size with film thickness. It was found that the crystallite sizes are increasing with increase of the film thickness.

3.4. Electrical properties

3.4.1. I–V characteristics

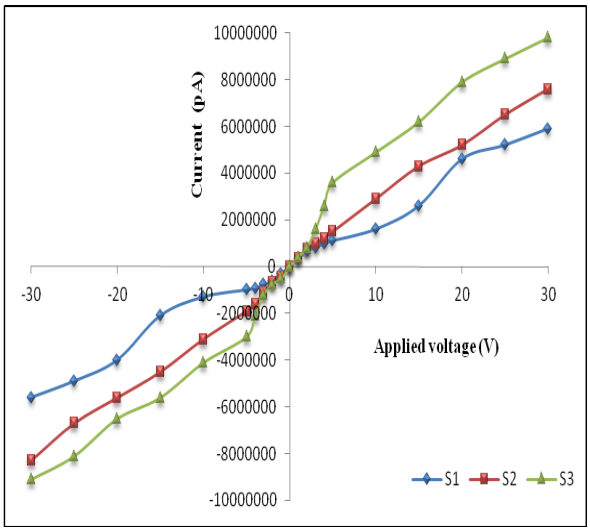

Fig. 7. I–V characteristics of nanocrystalline SnO_2 thin film sensors.

Fig. 7 shows the I–V characteristics of samples S1, S2, and S3 observed to be nearly symmetrical in nature indicating ohmic nature of contacts. The non-linear I–V

characteristics may be due to semiconducting nature of the films. S1, S2, and S3 are the films obtained by spraying for concentration of solution: 0.025M, 0.050M, and 0.075M respectively.

3.4.2. Electrical conductivity

Fig. 8 shows the variation of log (conductivity) with operating temperature. The conductivity of each sample is observed to be increasing with an increase in temperature. The increasing of the conductivity with increase of temperature could be attributed to negative temperature coefficient of resistance and semiconducting nature of nanocrystalline SnO_2.

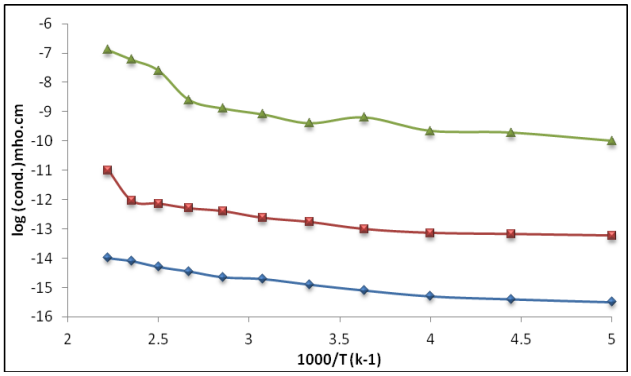

Fig. 8. Variation of log (conductivity) with operating temperature (◦C).

It is clearly indicates that the nanocrystalline SnO_2 thin films are semiconducting in nature. It is reported [14-15] that when thickness of the film increases activation energy goes on decreases. In Table 2 the activation energy calculated from slopes of line for 0.025M, 0.050M, and 0.075M thin films were found (200 - 400 ^oC) to be 0.61eV, 0.56 eV, 0.56 eV, 0.051 eV, 0.43 eV and 0.31 eV respectively.

Table 2. Measurement of activation energy and film thickness.

Sample No.	Thickness (nm)	Activation energy ($\triangle$ E)	
		200 ^OC	400 ^OC
S1	180	0.61 eV	0.56 eV
S2	210	0.56 eV	0.51eV
S3	289	0.43 eV	0.31eV

It is clear from Table 2 that, as film thickness of the sample goes on increasing; the activation energy goes on decreasing. The decrease in activation energy with increasing film thickness may be due to the change in structural parameters, improvement in crystalline and grain size [16].

3.5. Gas sensing performance of the sensors

3.5.1. Measurement of response

Gas response (S) of the sensor is defined as the ratio of change in conductance of sensor to its conductance exposure of target (at same operating conditions).

$$S = Gg – Ga / Ga \quad (5)$$

where, Ga = the conductance of the sensor in air
Gg = the conductance on exposure of a target gas.

3.5.3. Effect of operating temperature on the sensor:

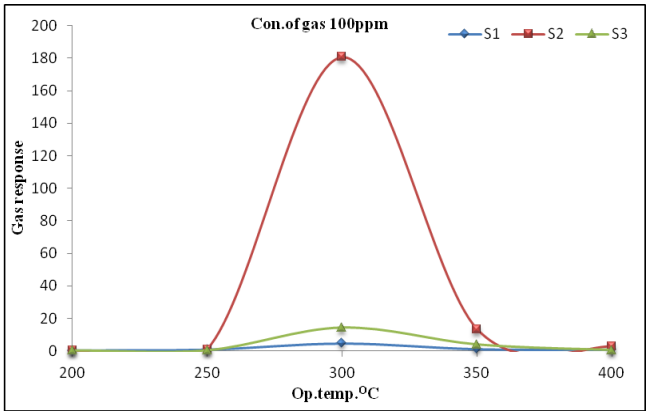

Fig. 9. Gas response of pure nanocrystalline SnO_2 thin films with operating temperature.

For the present work, initially the gas response was studied as a function of operating temperature for a SnO_2 thin film (for concentration of solution from 0.025M - 0.075M upon) exposure to 100 ppm of CO gas. It is clear from Fig. 9, that the gas response reaches maximum at 300^oC (gas response = 180.81) and then decreases at 350 ^oC. Therefore the temperature of 300^oC was taken as an optimum operating temperature for further studies.

3.4.4. Selectivity of CO for SnO2 thin films for various gases

Fig. 10 shows the histogram of the selectivity of nanocrystalline SnO_2 thin films to various gases. The table attached to histogram shows the gas response values to various gases at different concentration of precursor solution. The films showed highest selectivity for to CO (Carbon monoxide = 100 ppm) against all other tested gases: LPG (Liquified petroleum gas), CO_2 (Carbon dioxide), H_2 (Hydrogen), NH_3 (Ammonia), C_2H_5OH (Ethanol) and Cl_2 (Chlorine).

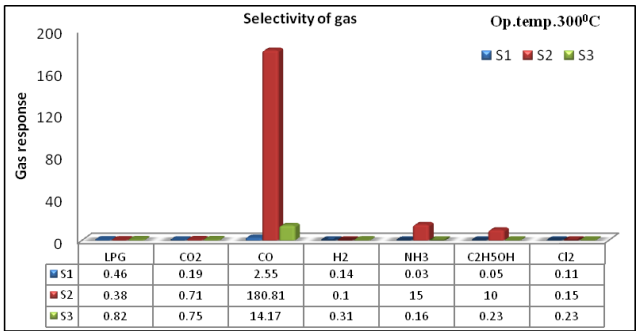

Fig. 10. Selectivity of nanocrystalline SnO_2 thin films for different gases.

3.4.5. Response and recovery of the sensor

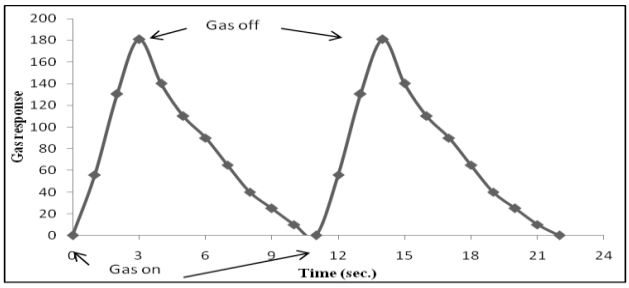

Fig . 11. Response and recovery of the sensor.

Table 2. Response and recovery characteristics for 100 ppm of CO.

Concentration of solution	Gas response	Response time (sec.)	Recover time (sec.)
0.025M	2.55	2	9
0.050M	180.81	3	8
0.075M.	14.17	5	18

The time taken for the sensor to attain 90% of the maximum decrease in resistance on exposure to the target gas is the response time. The time taken for the sensor to get back 90% of original resistance is the recovery time. The response and recovery of the nanostructured SnO_2 thin film (S2) sensor on exposure of 100 ppm of CO at 300^oC are represented in Fig. 11. The response is quick (3 s) and recovery is fast (8 s). The high oxidizing ability of adsorbed oxygen species on the surface nanoparticles and high volatility of desorbed by-products explain the quick response to CO and fast recovery. Table 2 shows the response and recovery time of all the samples to CO at 300 ^oC.

3.4.6. Comparison of CO response of reported sensors with sensor prepared in the present work

Table 3 presents comparison of CO response with reported different sensor [17-22] and sensor prepared in present investigation.

Table 3. Comparision of CO response with previous work.

Form of material/ sensor	Gas conc.(ppm)	Gas response	Operating Temperature(^oC)	Reference
SnO_2 (Thin form)	100	180.81	300	Present work (Sample S2)
ZnO (Thin form)	200	9	300	[17]
SnO_2 (Thin form)	10	2.34	400	[18]
SnO_2 Grafted MCM (Thin form)	100	23	200	[19]
Commercial SnO_2 (Thin form)	100	7	400	[19]
TiO_2 (Thin form)	10	1.6	350	[20]
Au-SnO_2 (Thin form)	500	45	250	[21]
SnO_2 (Thin form)	1000	27	50	[22]

It is clear from Table 3 that, the response of sensor in the present investigations is more sensitive to CO in its pure form as compared to other sensors.

3.5. Discussion

3.5.1. Kinetics in thin film deposition

The deposition process needs fine droplets to react on the heated substrate, owing to the pyrolytic decomposition of the solution. The hot substrate provides the thermal energy for the thermal decomposition and subsequent recombination of the constituent species. In many cases large droplets of the solution do not vaporize before reacting to deposit on the substrate. They hit the surface and form a powdery deposit. If it strikes at a high enough velocity, the droplet will splatter and form a dispersed powdery layer. As mentioned above, the droplet cannot be completely vaporized before it hits the surface and for this reason, film growth cannot occur [23]. The influence of forces which determine both the trajectory of the droplets and evaporation were examined and a film growth model was proposed. Fig. 12 shows the types of trajectories that are expected to occur in the spraying of a solution on hot glass substrate. It is reported that the behaviour of precursor drops undergo three major steps during the course of spray pyrolysis: (i) drop size shrinkage due to evaporation, (ii) conversion of precursor into oxides, and (iii) solid particle formation. The particle formation may involve two mechanisms: intraparticle reaction (conventional one-particle-per-drop mechanism) and gas-to-particle conversion [24]. In the one-particle-per-drop mechanism, each droplet is regarded as a micro reactor and converts into one solid particle when it travels towards substrate. In contrast, gastoparticle conversion occurs when the precursor is volatile and is transported across the particle–gas interface.

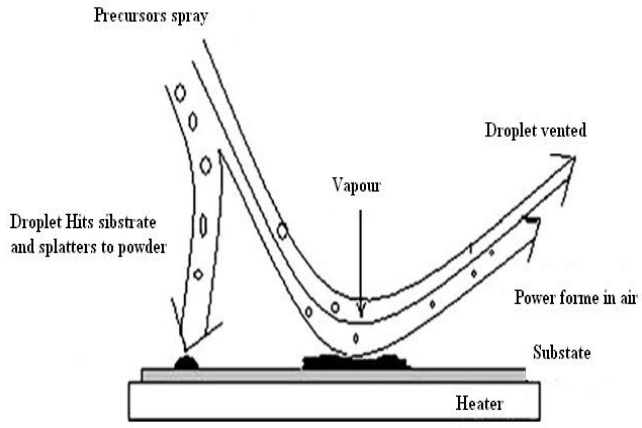

Fig. 12. Kinetics in thin film deposition.

The phenomenon for the preparation of a metal oxide thin film depends on surface hydrolysis of metal chloride on a heated substrate surface in accordance with the equation,

$$XCl_m + nH2O \rightarrow XO_n + mHCl \quad (5)$$

Where X is the metal such as Sn, Zn, Cu etc of the oxide films.

3.5.2. *Gas sensing mechanism*

It is important to maintain the SnO_2 phase during sensor operation, as a change would destroy or at least change the sensing properties. The gas sensing mechanisms of SnO2 is still not fully understood. However, the principle of operation of SnO_2-based sensor lies on detecting the conductivity changes experienced by an n-type material when surface chemisorbed oxygen reacts with reducing gases, such as CO, H_2S etc. In the detection mechanism, in clean air the conductivity of SnO_2 is low because the conduction electrons are bound to surface oxygen, whereas in the presence of a reducing gas, electrons are no longer bound to surface states and the conductivity increases. Therefore, the adsorption of gaseous species controls the resistance of the nanocrystalline SnO_2 as well as that of the grain boundaries. Receptor function concerns the ability of the oxide surface to interact with the target gas. The surface oxygen, especially adsorbed oxygen of the oxide acts as receptor. In air, oxygen is adsorbed on the oxide grains as negatively charged ion, inducing a surface space charge layer depletive of electrons or increasing the work function of the grains. When the grain size of the material is small enough, the material resistivity of the device is determined by the grain control and the material conduction type is surface conduction dominant [25-26], therefore grain size of the material is the one of the key factors to control the gas sensing properties of the material [27].

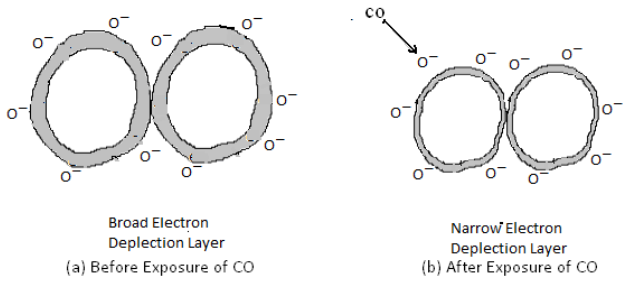

Fig. 13. Sensing mechanism of nanocrystalline SnO_2 thin film.

Fig. 13 shows the CO sensing mechanism (Fig. (a) before exposure of CO and (b) after exposure of CO) of nanocrystalline SnO_2 thin films. When the oxidation reaction rate of carbon monoxide is much higher than the rates of adsorption and desorption of the reactants, the

steady state oxygen coverage depends critically on the relative oxygen and CO concentrations in the gas phase. To allow for fast surface reactions the temperature has to be high enough, although not too high, to prevent bulk-surface interactions which can cause long time variations in the sensor parameters. Oxidation of carbon monoxide on a tin oxide surface may occur through many different reaction paths, depending on the surface composition, structure and temperature and on adsorbed species. Most of the time, the intermediates and complexes formed during reaction are short-living compounds that are not easily identified. However, in order to understand the overall sensing mechanism of carbon monoxide, it is necessary to know what oxygen species are present on the surface and their extent, how does CO adsorb on the surface, which reaction paths are possible and which is the rate of each step, what other elements may interfere in the reaction and if they are present. The response of the sensing materials is based on chemisorption, i.e. the exchange of charge between absorbed gases and the metal oxide surface. In air, there are several different negatively charged oxygen adsorbates, such as O^{2-}, O^{-}, and O^{2-}, which are known to cover the metal oxide surface. The formation of an oxygen adsorbate layer leads to a decrease in the electron density on the metal oxide surface due to charge transfer from the metal oxide to the adsorbate layer. When the metal oxide used as a sensing material is exposed to reducing gas molecules, the gas molecules are oxidized by the oxygen ions on the metal oxide surface, resulting in the release of free electrons to the metal oxide and, consequently, to an increase in the conductance (decrease of resistance) of the metal oxide. This implies that the gas sensing behavior of a metal oxide semiconductor is strongly related to its surface properties. Then, by varying the surface morphology, it is possible to tune the gas sensing properties of a material. Indeed, depending on surface properties of the nanocrystallites, a unique combination of structural, electronic, and adsorption/desorption process parameters can be obtained, thus the design of nanomaterials with controlled shape and/or morphology can participate to the enhancement of the sensing properties.

4. Conclusion

1) Nanocrystalline SnO_2 thin films could be prepared by simple and inexpensive spray pyrolysis technique.
2) The structural and microstructural properties confirm that the as-prepared SnO_2 thin films are nanocrystalline and spherical in shape.
3) Increase in thickness of the films was observed to increase in concentration of precursor solution.
4) Increase in concentration of precursor solution, texture coefficient for plane (110), (101) and (200) also increases.
5) Crystallite and grains size increased with increasing of film thickness.
6) The response of the nanocrystalline SnO_2 sensor was observed to be most sensitive to CO.
7) The sensor has good selectivity to CO against LPG, CO_2, H_2, NH_3, C_2H_5OH and Cl_2.
8) The nanostructured SnO_2 thin films exhibit rapid response–recovery which is one of the main features of this sensor.

Acknowledgements

The authors are thankful to the University Grants Commission, New Delhi for providing financial support. Thanks to Principal, G. D. M. Arts, K. R. N. Commerce and M. D. Science College, Jamner, for providing laboratory facilities for this work.

Reference

[1] S. M.A. Durrani, E. E. Khawaja M. F. Al-Kuhaili, Talanta, **65**, 1162 (2005).
[2] O. Wurzinger, G. Reinhardt, Sensors and Actuators B, **103**, 104 (2004).
[3] M. de la L. Olvera, R. Asomoza, Sensors and Actuators B **45**, 49 (1997).
[4] K. Murakami, K. Nakajima, S. Kaneko, Thin Solid Films, **515** 8632 (2007).
[5] T. Mochida, K. Kikuchi, T. Kondo, H. Ueno, Y. Matsuura, Sens. Actuators B **24**, 433(1995).
[6] L. A. Patil, M. D. Shinde, A. R. Bari, V. V. Deo, Sensors and Actuators B **143**, 270 (2009).
[7] T. Okuno, T. Oshima, S. Dong Lee, S. Fujita, Physica Status Solidi, **110**, 8540 (2011).
[8] H. S. Randhawa, M. D. Matthews, R. F. Bunshah, Thin Solid Films **83**, 267 (1981).
[9] T. Mohanty, Y. Batra, A. Tripathi, D. Kanjilal, J Nanosci Nanotechnol, **7** 2036 (2007).
[10] T. Gui, L. Hao, J. Wang, L. Yuan, W. Jai, X. Dong, Chineses Optics Letters **8**, S10134 (2010).
[11] J. Liu, S. Gong, J. Xia, L. Quan, H.Liu, D. Zhou, Sensors and Actuators B **138**, 289 (2009).
[12] ASTM card no.05-0467.
[13] S. D. Sartale, C. D. Lokhande, Materials Chemistry and Physics, **2**, 101 (2001).
[14] K. C. Sharma, J. C. Garg Phys. D: Appl. Phys **23**, 1411 (1990).
[15] Z. S. EL-Mandouh, M. EL-Shabasy, FIZIKAA **4**, 17 (1995).
[16] R. B. Kale, C. D. Lokhande, Semicond. Sci. Technol. **20**, 1 (2005).
[17] T. Krishnakumara, R. Jayaprakashb, N. Pinnac, N. Donatod, A. Bonavitae, G. Micalie, G. Nerie, Sensors and Actuators B, **143,** 198 (2009).
[18] Chang Sup Moona, Hae-Ryong Kima, Graeme Auchterlonie, John Drennan, Jong-Heun Lee, Sensors and Actuators B, **131**, 556 (2008).
[19] Guo Hua Gao, Sibudjing Kawi, Ming Yuan He, Sensor Chinese Chemical Letters, **16**, 1071 (2005).
[20] Youn-Ki Jun, Hyun-Su Kima, Jong-Heun Lee, Seong-Hyeon Honga, Sensors and Actuators B, **120**, 69 (2006).

[21] L. H. Qian, K. Wanga, Y. Lia, H. T. Fang, Q. H. Lua, X. L. Maa, **100**, 82 (2006).
[22] S. Mosadegh Sedghi, Y. Mortazavi, A. Khodadadi, O. Alizadeh Sahraei, M. Vesali Naseh, Sonochemically World Academy of Science, Engineering and Technology, **49** (2009).
[23] A. S. Gurav, T. T. Kodas, J. Joutsensaari, E. I. Kauppinen, R. Zilliacus, J. Mater. Res **10**, 1644 (1995).
[24] W. M. Sears, M. A. Gee, Thin Solid Films **165,** 265 (1998).
[25] L. A. Patil, A. R. Bari, M. D. Shinde, Vinita Deo, M. P. Kaushik, Sensors and Actuators B: Chemical, **161,** 372 (2002).
[26] L. A. Patil, A. R. Bari, M. D. Shinde, Vinita Deo, Sensors and Actuators B: Chemical, **149,** 79 (2010).
[27] G. Martinelli, M. C. Carotta, E. Traversa, G. Ghiotti, MRS Bull**. 6**, 30 (1999).

*Corresponding author: rameshbari24@yahoo.com